Contrasting depth distribution of colloid-associated phosphorus in the active and abandoned sections of an alluvial fan in a hyper-arid region of the Atacama Desert

Ghazal Moradi[ab], Roland Bol[a], Luka Trbojevic[a], Anna Missong[a], Ramona Mörchen[c], Barbara Fuentes[d], Simon M. May[e], Eva Lehndorff[c], Erwin Klumpp[a]*

[a] Agrosphere (IBG-3), Institute of Bio- and Geosciences, Forschungszentrum Jülich GmbH, Germany

[b] Institute for Environmental Research, Biology 5, RWTH Aachen University, Worringerweg 1, 52074 Aachen, Germany

[c] Institute of Crop Science and Resource Conservation - Soil Science and Soil Ecology, University of Bonn, 53115 Bonn, Germany

[d] Laboratorio de Tecnología de Membranas, Medio Ambiente y Biotecnología, Departamento de Ingeniería Química, Universidad Católica del Norte, Antofagasta, Chile

[e] Institute of Geography, University Cologne, Albertus-Magnus-Platz, 50923 Cologne, Germany

*** Corresponding author: Ghazal Moradi, g.moradi@fz-juelich.de, Tel: +49 (0)2461613521**

ABSTRACT

Colloids and their subset nanoparticles are key soil constituents for nutrient and organic carbon (OC) storage and transport, yet little is known about their specific role in overall transfer of elements under hyper-arid conditions. We analyzed the Water Dispersible Colloids (WDCs) of two adjacent soil profiles, located either on the active (named: Fan) or passive (named: Crust) sections of an alluvial fan. Colloidal particles (<500 nm) were fractionated using Asymmetric Field-Flow-Field Fractionation (AF^4), which was coupled online to an Inductively Coupled Plasma-Mass Spectrometer (ICP-MS) and an Organic Carbon Detector (OCD) to detect the composition of size-fractionated colloids. Three size categories of particles were identified: nanoparticles (0.6-24 nm), fine colloids (24-210 nm), and medium colloids (210-500 nm). The two profiles differed distinctively in vertical WDC distribution and associated phosphorus (P) content. Fractograms of the Crust profile predominantly showed fine colloids, whereas the medium-sized colloids dominated those of the Fan. Furthermore, the highest colloid content in the Crust profile was found at the surface, while in the Fan, colloids accumulated at 10-20 cm depth, thus overall reflecting the different genesis and infiltration capacities of the soils. Despite very low concentration of colloidal P in these hyper-arid soils, a strong correlation between colloidal P and calcium (Ca), Silica (Si), aluminum (Al), iron (Fe), and OC content were found. This also revealed Ca-phosphates as the primary P retention from, with the association of P to phyllosilicates and Fe/Al (hydr-) oxides as the main soil colloidal fractions. Overall, our results did highlight that small local scale differences in topographic-derived distribution of water flow pathways, defined the formation of the crust-like surfaces, and ultimately the overall movement and distribution of nanoparticles and colloids in soil profiles under hyper-arid conditions.

Keywords: Hyper-arid soils, Water dispersible soil colloids, Phosphorus, Field-Flow-Field-Fractionation

INTRODUCTION

Soil colloids (1-1000 nm) and nanoparticles (<100 nm) have high specific surface areas due to their small size, and therefore high bonding capacity for nutrients, for example P (Molina, 2016; Gottselig et al., 2017). Moreover, soil colloids are highly mobile, and hence promote the transport of the adsorbed nutrients in the environment (Wilkinson and Lead, 2007). For this reason, many studies have been conducted to examine P associations to colloidal particles in forest soils (Bol et al., 2016; Missong et al., 2018), stream waters (Baken et al., 2016; Gottselig et al., 2014, 2017) as well as in arable soils (Jiang et al., 2015; Séquaris et al., 2013). Nevertheless, little attention has been paid so far to this small yet likely important pool in soils of the arid systems.

The Atacama Desert, northern Chile, is known to be the most water-deficient environment on the planet. However, under the influence of the El Niño Southern Oscillation (ENSO), intense winter rainfalls might occur in the Pacific coastal regions (Houston, 2006). Although in the current century, the climate has become drier in the Atacama, the number of irregular rain events has increased (Ortega et al., 2019). Some of these rainfall events might be effective for the *in-situ* translocation of the soil colloidal particles into the subsurface. Moreover, in the most extreme cases, a differential preferential (sub)surface flow pathway, resulting from small scale topographical variations, might further influence the key genesis processes that can determine soil colloid distribution. The presence/absence of a surface crust, i.e. a hardened layer different from the rest of the soil, has been confirmed to affect the rate of infiltrating rainwater (Zhuang et al., 2009). Surface salt crusts composed of salt-cemented soil particles are important physical features of the Atacama soils, and formed by the accumulation of salts at the surface due to the upward capillary movement of water and vapor derived from evaporation (Amit & Yaalon, 1996; Amundson et al., 2008; Ewing et al., 2006). The surface crusts can protect the underlying soil against erosion (Jury & Horton, 2004), and therefore, their absence may promote more leaching of colloidal particles to deeper layers (Davis et al., 2010).

Natural soil colloids and nanoparticles are typically found in soils in the form of phyllosilicates, Fe/Al (hydr-) oxides, and organic colloids. However, manganese (Mn) oxides, metal sulfides, carbonates, phosphates, and amorphous SiO_2 can also occur in the size range of natural soil colloids (Missong et al., 2018b; Wilkinson and Lead, 2007). All the above-mentioned soil

colloids can occur independently in the soils, or they can be involved in the complex association of the colloidal matter in which soil pH plays a significant role in the final colloidal structure. At about pH <8, Fe and Al (hydro) oxides have a positive surface charge and thus can also bind anions. Cations however, preferentially adsorb to organic and inorganic soil colloids, such as soil organic matter and phyllosilicates, respectively.

Phosphorus is an irreplaceable nutrient for the existence of life on earth (Black, 1957) and can bind to organic and inorganic soil colloids and nanoparticles. This process is also controlled primarily by the pH value of the soil. In acidic soils, phosphate ions are primarily fixed on iron, aluminum, and manganese (hydro) oxides, but they can also be attached to the surface of phyllosilicates. In alkaline soils, on the other hand, phosphorus is often present in the form of calcium phosphates. Organic soil colloidal particles may also be associated with phosphate or organic phosphate compounds. However, due to the negative surface charge of the organic colloids and nanoparticles, the bond is only via Al/Fe bridges in an acidic medium and over Ca/ magnesium (Mg) bridges in an alkaline environment (Dolfing et al., 1999; Makarov & Malysheva, 2006).

The P distribution and association to other soil compartments is rarely studied in hyper-arid and arid climates of the Atacama. Fabre et al. (2006) found considerable amounts of labile P in the soils of different Lomas vegetation in the hyper-arid Atacama in Peru. These investigated soils had also elevated organic carbon contents compared to the soils of other regions in the Atacama Desert (Mörchen et al., 2019). Elevated organic carbon contents were also found in the Mediterranean climatic zone of Chile, in which P association was confirmed in connection with Fe, Al oxides and organic material at acidic pH conditions (Borie and Zunino, 1983). However, we are not aware of any study so far that unraveled the colloidal P distribution and association in organic carbon poor environments with minimum water availability, such as in the hyper-arid region of the Atacama with alkaline soils (Ewing et al., 2008; Ewing et al., 2006). The main objective of this study was to investigate and compare the vertical distribution of the colloidal particles and their P content in the active and abandoned sections of an alluvial fan in a hyper-arid region of the Atacama.

2. MATERIALS AND METHOD

2.1. Study area and sampling

The study area is located near Paposo in the south of Antofagasta about 13.5 km from the Pacific coast (25°00′55.84″ S 70°20′15.23″W) (Fig. 1a). The average annual temperature is between 17.2 °C, and the mean annual precipitation is <0.1 mm/year (Quade et al., 2007). The dry index is 0.20 indicating an extreme soil moisture deficit in this zone (Houston and Hartley, 2003; Quade et al., 2007). The geological substrate is loose, unconsolidated silica-rich material of magmatic origin (Quade et al., 2007) with a sandy to coarse rock grain size (Fig. 3). There is no sign for a horizon differentiation due to soil forming processes such as the precipitation of gypsum or calcite so that the soils can be defined as Regosols (WRB, 2014~~).~~

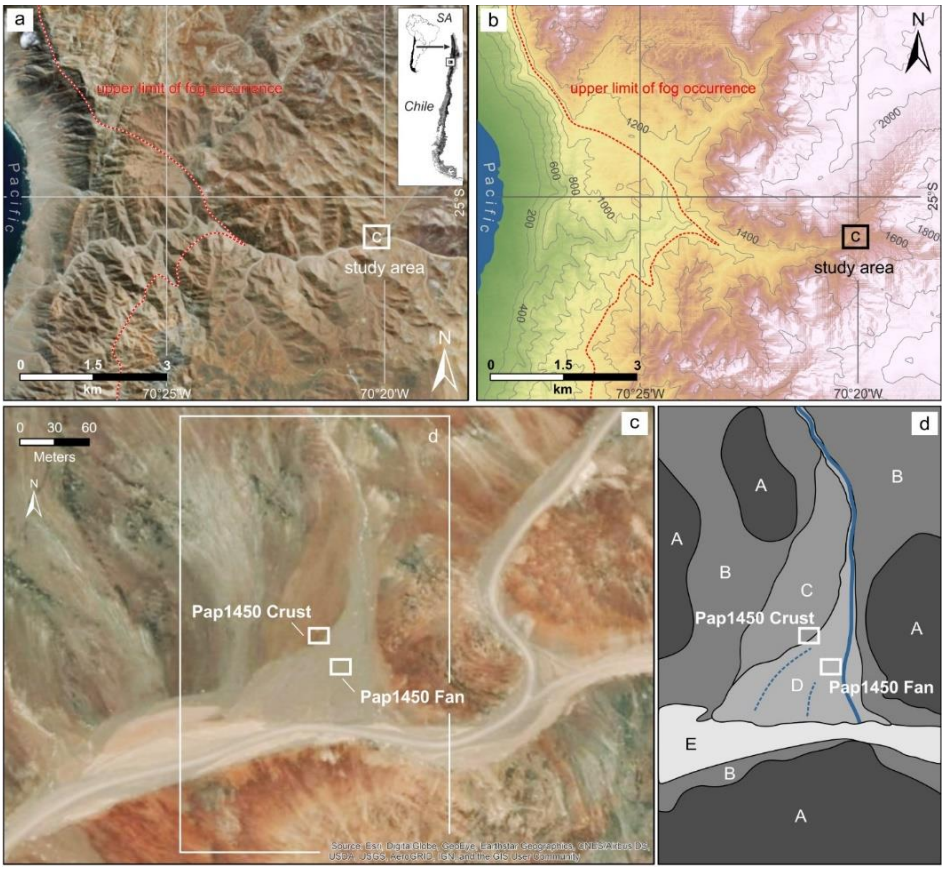

Fig. 1- Study area. *(a) Location of the study area at the elevation of 1450 m.a.s.l. (c) position of soil profiles on a fan, showing the two different alluvial fan sections, with red colors dominating the abandoned surface, and gray to brown colors indicating the younger and active fan sections. (a & c) are based on ArcGIS 10.5 background imagery (Esri, DigitalGlobe, GeoEye, i-cubed, USDA FSA, USGS, AEX, Getmapping, Aerogrid, IGN, IGP, swisstopo und die GIS User Community, see also note in (c). (b) Digital elevation model of the area shown in (a) based on ALOS Global Digital Surface Model (AW3D30); original data is provided by the Japan Aerospace Exploration Agency (JAXA); the upper limit of fog bank is typically around 1100 m. (d) Geomorphology units of the study sites: A– Bedrock, B- Hillslope deposits / scree deposits, C- older (inactive) alluvial fan generation, D- younger (active) alluvial fan generation, E- modern flood plain.*

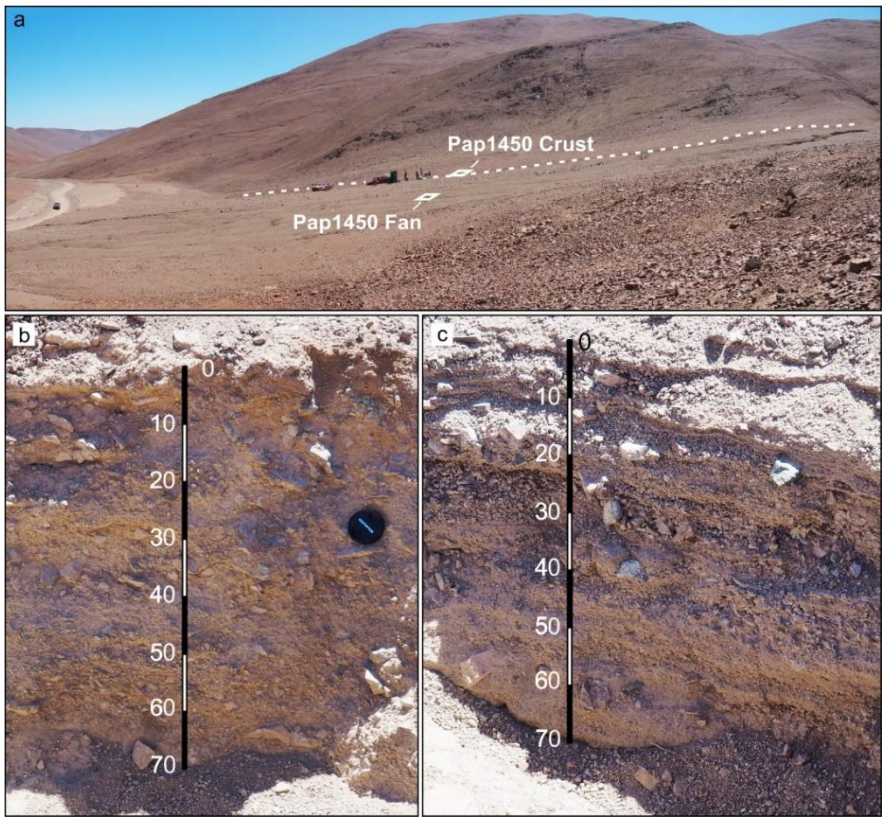

Fig. 2*- Soil profiles. (a) Position of the profiles on the fan surface. (b) and (c) show the Crust and Fan profile, respectively.*

The soil samples were taken in October 2016 from a site at an elevation of 1450 m a.s.l located on an 80 m wide and ~200 m long alluvial fan system (site Pap1450) (Fig. 1). Two profiles with a depth of 70 cm were dug in the direct vicinity of each other: the profile named Pap1450-Crust is located on the abandoned (passive) fan surface, which was indicated by reddish sediment colors, indurated sediment layers, and a rather solid/hard crust-like surface (Fig. 2b). The other profile named Pap1450-Fan was dug some few meters downslope of Pap1450-Crust, in the center of the presently active fan surface (Fig. 2c). Grey colors, rather loose bedding, and a distinct stratigraphy with well-defined layers of different grain size characterize the younger fan surface and subsurface sediments. The abandoned and currently active fan sections are separated by a ~0.8 m-high topographical step (Fig. 1b), which indicates a multi-phase evolution of the fan system related to incision of the younger, active fan section. While absolute ages of the different fan generations are not available, the different characteristics of surface and subsurface

sediments (e.g., clay and silt contents; Fig. 3) suggest that the upper fan section with profile Pap1450-Crust is considerably older, i.e. abandonment of the fan section may have occurred during the late Pleistocene or early to mid-Holocene. Samples were taken without regard to soil horizons from each 10 cm to have a better resolution of the distribution of colloids and colloidal P. Each sample was a composite sample from several points of the same layer, and special care was taken to avoid losing very fine particles in the course of sampling. There was no viable vegetation in the studied area at the time of sampling. However, few dry shrubs were observed on top of the younger fan surface.

2.2. Total P content and soil texture

One gram of the air-dried, sieved and ground soil was mixed with 7 ml of a 65% HNO_3 solution and 21 ml of a 37% HCl solution in a mixing ratio of 3:1. The digestion itself was carried out after reaching the boiling point of 160 °C, in which the aqua regia remained for two hours. Finally, the content of P in the aqua regia extracts was quantified by Inductively Coupled Plasma Optical Emission Spectroscopy (ICP-OES).

Soil texture analysis was also done via combined sieving and pipetting based on the protocol of the International Organization for Standardization (ISO 11277, 2002).

2.3. WDCs extraction and consequent Field Flow Field Fractionation

The WDCs were extracted according to the method of (Séquaris & Lewandowski, 2003). Six gram of each sample (d <2 mm) was mixed with deionized water with a ratio of 1:2 (soil:water) and shaken for 6.5 h on a horizontal shaker at 150 rpm. The suspension was then diluted 4-fold with deionized water and left to sediment for about 6 min to remove the fractions larger than 20 μm (Sedimentation time was calculated using Stokes' law). The supernatant was removed by using a pipette, and after that, the suspension containing particles <20 μm was centrifuged for about 7 min at 4000 rpm. The centrifugation time was calculated according to Hathaway (1956) in order to obtain the WDC with particle sizes <500 nm in the supernatant. The extraction procedure was applied equally to all samples. Moreover, offline Dynamic Light Scattering measurements (DLS) were performed to approve the validity of the extraction procedure (Table S1).

Extracted WDCs were fractionated by size using AF^4 (AF2000, Postnova Analytics, Landsberg, Germany). The parameters of the AF^4 separation method were shown in Table S2. The AF^4 was coupled online with an ICP-MS (Agilent 7500, Agilent Technologies), as well as OCD. The content of OC was measured with the OCD and the content of Si, Fe, Al, Ca and P by ICP-MS. The detection limit was 0.1 mg L^{-1} for P, 0.01 µg L^{-1} for Al, 3.3 µg L^{-1} for Si, 0.02 µg L^{-1} for Fe, and 0.1 µg L^{-1} for Ca (Missong et al., 2018).

The conversion of separation time to the relevant particle size was done by analyzing latex standards (from Postnova analytics) under the same conditions as the samples. The quantification of ICP-MS/OCD-AF^4 was done by external multipoint calibration.

2.4- Statistical analysis

Bravais-Pearson correlation analysis was performed using Microsoft Excel 2013. The significance of the correlations was also tested by regression test. All the figures were also prepared using OriginPro 2017.

3. RESULTS

3.1. Size of the fractionated WDCs

The resulting fractograms from the online-coupling of AF^4 to ICP-MS and OCD depict the occurrence of three distinct peaks for all the samples (Fig. S1 and S2). Fractograms of the two surface layers (0-10 cm) were chosen to illustrate the three distinct classes of size-fractionated WDCs (Fig. 4). Based on the size calibration of latex standards, the first and second peaks were associated with nanoparticles and fine colloids with the size of 0.6-24 nm and 24-210 nm, respectively. The last eluting particles of the third peak (‘release peak’ described by (Neubauer et al., 2013) in the range of 210 to 500 nm were titled medium colloids (Fig. 4). Based on the off-line DLS measurements (Table S1), the extracted WDCs of the Fan profile were on average (23%) larger than the Crust which can be seen to be reflective of the general dominance of the third peak (medium sized colloids) in the former ICP-MS/OCD-AF^4 fractograms (Fig. S1).

3.2. Elemental composition of WDCs

The peak areas of ICP-MS-AF^4 fractograms were quantified to obtain the inorganic elemental contents of the size-separated WDCs reflecting the distribution of WDCs (Fig.5). In the Crust, the maximum element contents were observed at the surface with a general decreasing trend

towards the deeper parts (Fig. 5). In this profile, Si, Fe, and Al dominated the composition of WDCs with the highest values of 501 mg kg^{-1}_{soil}, 192 mg kg^{-1}_{soil} and, 190 mg kg^{-1}_{soil}, respectively

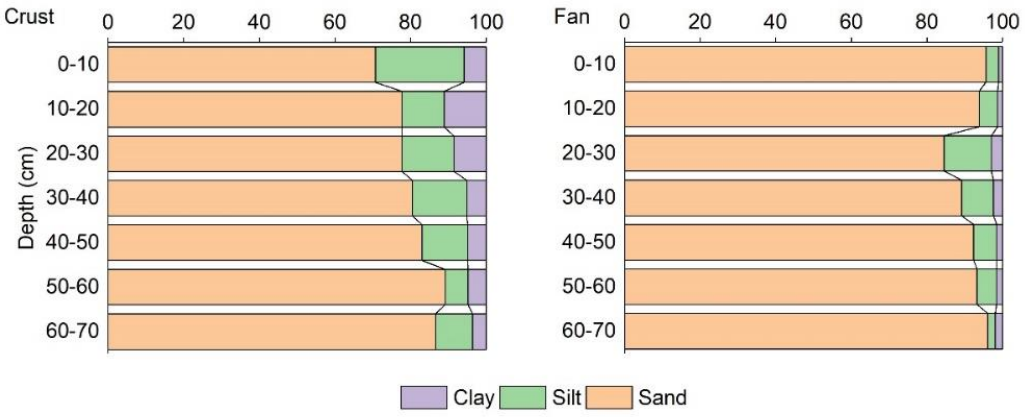

Fig. 3- *Soil texture. The percentage of sand, silt, and clay are illustrated.*

(Table S1). Moreover, Ca content ranged from 30.8 to 6.7 mg $kg^{-1}_{soil,}$ presenting the general decreasing trend from top to bottom. Unlike the Crust, the maximum concentrations in the Fan except for P and Ca were found at a depth of 10-20 cm, and the lowest ones at 50-60 cm (Table S1). The highest content of Si, Fe, and Al were 2-3 times smaller than the Crust with values of 159 mg kg^{-1}_{soil}, 73.5 mg kg^{-1}_{soil}, and 55.5 mg kg^{-1}_{soil}, respectively.

The quantification of the AF^4-OCD fractograms showed a fairly similar distribution of the organic in comparison to inorganic colloidal components across the soil profiles (Fig. 5). The WDC OC concentrations ranged from 5.1 to 0.5 mg kg^{-1}_{soil} in the Crust and from 2.1 to 0.6 mg kg^{-1}_{soil} in the Fan profile (Table S1). There was a significant positive correlation between colloidal OC content and the other measured colloidal elements in the Crust; however, in the Fan, this correlation was not statistically significant (Table 1). Both profiles did not show a significant relationship between colloidal and bulk OC contents. Nevertheless, this correlation was much stronger in the Crust ($p < 0.05$; R^2 were 0.08 and 0.4 for the Fan and Crust, respectively).

The overall composition of nanoparticles varied from that of fine and medium colloids in both investigated profiles (Fig. 5 and Table S1). Apart from nanoparticulate fractions in which Ca and Si were the prevailing inorganic elements, Si, Fe, and Al were the principal constituents of the other two size fractions. Maximum element contents were observed in the fine colloids of the

Crust profile; however, in the Fan, medium-sized colloids had the highest element concentrations (Fig. 5).

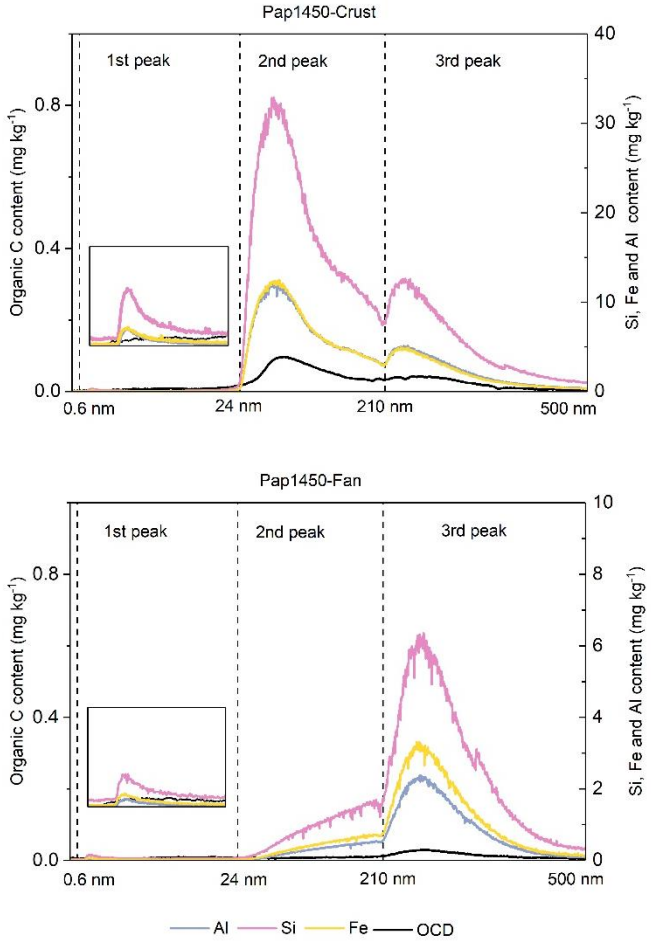

Fig. 4- *ICP-MS and OCD-AF^4 fractograms of the surface layer (0-10 cm) of the Crust and Fan profiles.*

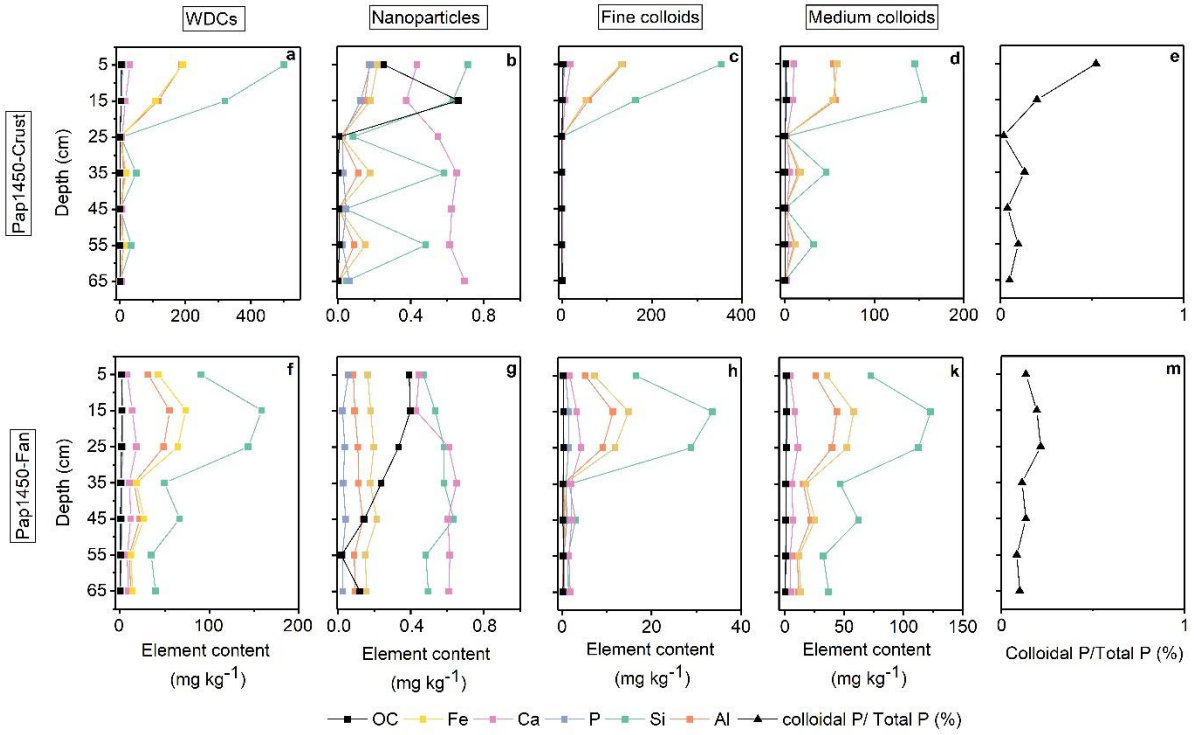

Fig. 5- *Elemental content of WDCs and their size fractions vs. soil depth. The illustrated data were obtained from the quantification of ICMPS/OCD-AF[4] fractograms. Elemental content of total WDCs, nanoparticles, fine and medium colloids of the Pap1450-Crust are shown in a, b, c, and d, respectively. Also, the panels named f, g, h, and k are respectively associated with the elemental content of WDCs, nanoparticles, fine and medium colloids in the Pap1450-Fan. All element contents are reported in mg kg$^{-1}_{Soil}$. The panels, e and m show the percentage of colloidal P to total P content in the Crust and Fan, respectively.*

3.3. P content and association in the WDCs

While the average P content of the Crust was only slightly lower than that of the Fan, the main difference was its depth distribution in the profiles (Fig. 5). In general, the distribution of P contents was comparable to that of other elements (Fig. 5). The Bravais-Pearson correlation coefficient ($p < 0.05$) was determined to investigate the correlation of colloidal P content to other measured colloidal elements and further statement about the P-associations (Table S3). In both profiles, colloidal P content significantly correlated to that of Ca, Si, Al, and Fe (Tables 1). However, there was a contrast between the profiles in terms of the correlation between the P and

OC contents of the fractionated WDCs, which was not statistically significant in Fan unlike the Crust profile (Table S3).

Table 1- *Correlations between WDCs elemental concentrations. Also, correlation coefficients between the WDCs element contents and the P content of nanoparticles, fine and medium colloids are given. Significant correlations are indicated by an Asterisk.*

		NP-P	*FC-P*	*MC-P*	*Al*	*Si*	*P*	*Ca*	*Fe*	*OC*
Pap1450-Crust	NP-P	1								
	FC-P	0.94	1							
	MC-P	0.45	0.65	1						
	Al	0.96*	0.99*	0.58	1					
	Si	0.96*	0.98*	0.58	1.00*	1				
	P	0.94*	1.00*	0.67	0.99*	0.99*	1			
	Ca	0.93*	1.00*	0.66	0.98*	0.98*	0.99*	1		
	Fe	0.96*	0.99*	0.60	1.00*	1.00*	0.99*	0.99*	1	
	OC	0.98*	0.96*	0.48	0.99*	0.99*	0.96*	0.95*	0.98*	1
		NP-P	*FC-P*	*MC-P*	*Al*	*Si*	*P*	*Ca*	*Fe*	*OC*
Pap1450-Fan	NP-P	1								
	FC-P	0.08	1							
	MC-P	0.07	0.98	1						
	Al	0.17	0.90*	0.84*	1					
	Si	0.16	0.91*	0.84*	1.00*	1				
	P	0.10	1.00*	0.98*	0.92*	0.92*	1			
	Ca	-0.07	0.90*	0.90*	0.75	0.77*	0.90*	1		
	Fe	0.20	0.88*	0.81*	1.00*	1.00*	0.90*	0.73	1	
	OC	0.38	0.70	0.60	0.91*	0.90*	0.74	0.51	0.93*	1

The overall apportionment of P between size-separated WDCs was similar in the two profiles, with the lowest P contents observed in nanoparticles (mostly below the detection limit) and the highest in fine colloid factions (Table S1). The Bravais-Pearson correlation analysis was also performed in order to comprehend the relationship between the P content of each colloidal fraction and the elemental content of total WDCs (Table 1). In this regard, the two profiles were dissimilar as in the Crust, the P content of medium colloids was not correlated to WDC contents of Si, Fe, Al, and OC, etc., while in the Fan the correlations were not significant for nanoparticulate fractions (Table 1).

4. DISCUSSION

Generally, the two soil profiles varied in terms of several factors that can eventually affect the depth profile of WDCs. First, different apportionment of WDCs between the two profiles (Fig. 5) is most likely to reflect in-situ translocation of colloidal particles due to topographic changes, that might happen in the (rare) event of the exceptional high-intensity rainfalls, e.g. occurring during El Nino phases of the ENSO cycle (Houston, 2006; Williams et al., 2008). Asymmetric distribution of rainwater and sediments on fluvial fans was shown in field experiments to result in spatially heterogeneous soil properties and vegetation cover (Mohseni et al., 2017). Therefore, the first justification for the contrasting WDCs distribution between the two profiles might be the topographic variations on the alluvial fan surface. Second, *in-situ* vertical colloid release and transport might also occur by the shear force imposed by the mechanical energy of the resulting infiltrating and draining rainwater, acting in the flow direction (Jonge et al., 1998; Schelde et al., 2002). Lack of the surface crust in the younger fan sections (Fan profile) might lead to higher infiltration rate compared to the Crust site. Apparently the lack of surface crust in of Fan site is due to ongoing activity by episodic fluvial processes, and in comparison, crust formation is a result of increasing surface age in the Crust (i.e., duration of surface inactivity). This means that for Paposo and possible the wider Atacama region, the morphodynamic inactivity of surfaces determines crust evolution and thus the depth distribution of colloids. The diminishing effect of the crust on infiltration rate was shown by Davis et al., (2010) with in-situ rain experiments in the Yungay area. Besides the sealing impact of the surface crust, the coarser soil texture of the active fan section (Fig. 3) provides larger pore space that also facilitates the removal of finer soil colloids by promoting rainwater infiltration (Lal and Shukla, 2004). The higher the flow rates, the more the colloid mobilization as a result of the elevated shear forces (Shang et al., 2008; Zhuang et al., 2007). However, Liu et al., (2013) showed that even under lower flow rates typical for semiarid regions, regardless of the amount of colloidal particles, colloids can be continuously transported into deeper soil layers.

The prevalence of medium-sized colloids (3rd peak) in the Fan profile and fine colloids (2^{nd} peak) in the Crust profile could be also associated to the eradication of finer fractions by fluvial activity and also infiltrating rainwater at the Fan site. Lack of the cementing soil organic matter as an intrinsic property of the desert soils reduces soil resistance to the shear forces (Andersland et al., 1981). Also, the low ionic strength of rainwater enhances the transport of colloids

(Makselon et al., 2018). Moreover, alkaline soil conditions might also enhance the colloid release due to the potential dissolution of organic material (Liang et al., 2010). However, the high electrolyte concentration generally supports the aggregation and hetero-aggregation (Séquaris et al., 2013; Tombácz et al., 2001) resulting in the formation of larger colloids. It was reported recently that fine and medium-sized soil colloids themselves are heteroaggregates consisting of nanosized soil components (Liang et al., 2015).

The size-resolved composition of WDCs (<500 nm) is a determining factor for P association to colloidal particles. The nanoparticles of both profiles were dominated by Ca and Si in all depths (Fig. 5) which is inconsistent with the composition of nanoparticles determined in acidic soils (Jiang et al., 2015; Missong et al., 2018). Our investigated soil was devoid of plant vegetation and did not contain significant amounts of organic matter (Mörchen et al., 2019). Therefore, it was not unexpected to observe that the OC content is not prevalent in the nanoparticles size fraction. Overall, it seems that in the investigated soils, the natural nanoparticles did not play an important role in the P fixation (mostly P contents of nanoparticles were below the detection limit, Table S3).

The dominance of Si, Al, and Fe in the fine and medium-sized colloids of both profiles could be indicative of phyllosilicates, Fe, and Al oxides (Tsao et al. 2011). Hyper-arid soils generally have low clay contents, but it has been shown that clay minerals (smectite, chlorite, and kaolinite) can be added to these soils by atmospheric dust deposition, and further move to deeper soil layers (Ewing et al., 2006). Preliminary XRD measurements of the samples did show the existence of chlorite. The fact that the Si/Al ratios were larger than two does suggest that, apart from clay minerals, sand-derived particles of colloid size might exist in these colloidal fractions (Rickson, 2012). The presence of phyllosilicates, Al- and Fe oxides as fine colloids and their association with P have also been reported for other soils (Jiang et al., 2015; Missong et al., 2018). In alkaline soils, P is mostly retained by direct interaction with Ca forming insoluble Ca-P salts (Turner et al., 2004). However, strong correlations between OC, P, and Ca in the Crust might reflect the association of OC and P via Ca bridges (Dolfing et al., 1999). A strong association of P to fine and medium colloids containing Si, Al, and Fe results in the translocation of P with the particles on which it is adsorbed (Table 1). Therefore, the colloidal P to total P ratio (Fig.5 e and m) follows the same trend as colloidal element contents of the distribution profiles under the

influence of the above-explained factors. However, further detailed investigations (e.g., field irrigation experiments) would help to better define the linkages between precipitation intensity, infiltration rates, and mineralogy of translocated associated P in soil colloids in these extremely arid environments.

5. CONCLUSION

The overall movement and distribution of nanoparticles and colloids in soil profiles under hyper-arid conditions is affected by the formation of the (physical) crust-like surfaces as a result of small scale differences in topographic-derived distribution of (occasional) water flow pathways. This different distribution of the nanocolloidal particles may affect the dynamics and element biogeochemistry of the alluvial fan.

ACKNOWLEDGMENTS

This work was done as part of a Collaborative Research Center project: 'Earth-Evolution at the Dry Limit,' funded by the Deutsche Forschungsgemeinschaft (DFG, German Research Foundation) – Projektnummer 268236062 – SFB 1211. The authors would like to thank Prof. Dr. Wulf Amelung for his valuable comments.

Data availability

The authors declare that all relevant data to the findings of this study are included in the paper and its supplementary information file.

REFERENCES

Amit, R., Yaalon, D.H., 1996. The Micromorphology of Gypsum and Halite in Reg Soils—the Negev Desert, Israel. Earth Surface Processes and Landforms 21, 1127–1143. https://doi.org/10.1002/(SICI)1096-9837(199612)21:12<1127::AID-ESP656>3.0.CO;2-G

Amundson, R., Ewing, S., Dietrich, W., Sutter, B., Owen, J., Chadwick, O., Nishiizumi, K., Walvoord, M.A., McKay, C., 2008. On the in situ aqueous alteration of soils on Mars. Geochimica et Cosmochimica Acta 72, 38453864. https://doi.org/10.1016/j.gca.2008.04.038

Andersland, O.B., Khattak, A.S., Al-Khafaji, A.W.N., 1981. Effect of Organic Material on Soil Shear Strength. Laboratory Shear Strength of Soil. https://doi.org/10.1520/STP28754S

Baken, S., Moens, C., van der Grift, B., Smolders, E., 2016. Phosphate binding by natural iron-rich colloids in streams. Water Res. 98, 326–333. https://doi.org/10.1016/j.watres.2016.04.032

Black, C.A., 1957. Soil-plant Relationships. Wiley.

Bol, R., Julich, D., Brödlin, D., Siemens, J., Kaiser, K., Dippold, M.A., Spielvogel, S., Zilla, T., Mewes, D., von Blanckenburg, F., Puhlmann, H., Holzmann, S., Weiler, M., Amelung, W., Lang, F., Kuzyakov, Y., Feger, K.-H., Gottselig, N., Klumpp, E., Missong, A., Winkelmann, C., Uhlig, D., Sohrt, J., von Wilpert, K., Wu, B., Hagedorn, F., 2016. Dissolved and colloidal phosphorus fluxes in forest ecosystems-an almost blind spot in ecosystem research. Journal of Plant Nutrition and Soil Science 179, 425–438. https://doi.org/10.1002/jpln.201600079

Borie, F., Zunino, H., 1983. Organic matter-phosphorus associations as a sink in P-fixation processes in allophanic soils of Chile. Soil Biology and Biochemistry 15, 599–603. https://doi.org/10.1016/0038-0717(83)90056-1

Davis, W.L., de Pater, I., McKay, C.P., 2010. Rain infiltration and crust formation in the extreme arid zone of the Atacama Desert, Chile. Planetary and Space Science 58, 616–622. https://doi.org/10.1016/j.pss.2009.08.011

Dolfing, J., Chardon, W.J., Japenga, J., 1999. ASSOCIATION BETWEEN COLLOIDAL IRON, ALUMINUM, PHOSPHORUS, AND HUMIC ACIDS. Soil Science 164, 171.

Ewing, S.A., Macalady, J.L., Warren-Rhodes, K., McKay, C.P., Amundson, R., 2008. Changes in the soil C cycle at the arid-hyperarid transition in the Atacama Desert. Journal of Geophysical Research G: Biogeosciences 113. https://doi.org/10.1029/2007JG000495

Ewing, S.A., Sutter, B., Owen, J., Nishiizumi, K., Sharp, W., Cliff, S.S., Perry, K., Dietrich, W., McKay, C.P., Amundson, R., 2006. A threshold in soil formation at Earth's arid-hyperarid transition. Geochemica et Cosmochimica Acta, Geochemicia et Cosmochimica Acta, Geochemimica et Cosmochimica Acta, GEOCHIM. COSMOCHIM. ACTA, GEOCHIM.COSMOCHIM.ACTA, Geochimica et Cosmichimica Acta, Geochimica et Cosmochica Acta, Geochimica et Cosmochimica, Geochimica et cosmochimica acta, Geochimica et Cosmochimica Acta,, Geochmimica et Cosmochimica Acta, Gochimica et Cosmochimica Acta, Goechimica et Cosmochimica Acta 70, 5293–5322. https://doi.org/10.1016/j.gca.2006.08.020

Fabre, A., Gauquelin, T., Vilasante, F., Ortega, A., Puig, H., 2006. Phosphorus content in five representative landscape units of the Lomas de Arequipa (Atacama Desert-Peru). CATENA 65, 80–86. https://doi.org/10.1016/j.catena.2005.10.004

Gauquelin, T., Puig, H., Ortega, A., Fabre, A., Vilasante, F., 2006. Phosphorus content in five representative landscape units of the Lomas de Arequipa (Atacama Desert-Peru). Catena 65, 80–86.

Gottselig, N., Bol, R., Nischwitz, V., Vereecken, H., Amelung, W., Klumpp, E., 2014. Distribution of Phosphorus-Containing Fine Colloids and Nanoparticles in Stream Water of a Forest Catchment. 1 - 11 0.

Gottselig, N., Nischwitz, V., Meyn, T., Amelung, W., Bol, R., Halle, C., Vereecken, H., Siemens, J., Klumpp, E., 2017. Phosphorus Binding to Nanoparticles and Colloids in Forest Stream Waters. Vadose Zone Journal 16, 0. https://doi.org/10.2136/vzj2016.07.0064

Hathaway, J.C., 1956. Procedure for Clay Mineral Analyses Used in the Sedimentary Petrology Laboratory of the U.S. Geological Survey*. Clay Minerals 3, 8–13. https://doi.org/10.1180/claymin.1956.003.15.05

Houston, J., 2006. Variability of precipitation in the Atacama Desert: its causes and hydrological impact. International Journal of Climatology 26, 2181–2198. https://doi.org/10.1002/joc.1359

Houston, J., Hartley, A.J., 2003. The central Andean west-slope rainshadow and its potential contribution to the origin of hyper-aridity in the Atacama Desert. International Journal of Climatology 23, 1453–1464. https://doi.org/10.1002/joc.938

Jiang, X., Bol, R., Nischwitz, V., Siebers, N., Willbold, S., Vereecken, H., Amelung, W., Klumpp, E., 2015. Phosphorus Containing Water Dispersible Nanoparticles in Arable Soil. J. Environ. Qual. 44, 1772–1781. https://doi.org/10.2134/jeq2015.02.0085

Jonge, H. de, Jacobsen, O.H., Jonge, L.W. de, Moldrup, P., 1998. Particle-facilitated transport of prochloraz in undisturbed sandy loam soil columns. Journal of environmental quality.

Jury, W.A., Horton, R., 2004. Soil Physics. Wiley.

Lal, R., Shukla, M.K., 2004. Principles of Soil Physics. CRC Press.

Liang, X., Liu, J., Chen, Y., Li, H., Ye, Y., Nie, Z., Su, M., Xu, Z., 2010. Effect of pH on the release of soil colloidal phosphorus. J Soils Sediments 10, 1548–1556. https://doi.org/10.1007/s11368-010-0275-6

Liu, Z., Flury, M., Harsh, J.B., Mathison, J.B., Vogs, C., 2013. Colloid mobilization in an undisturbed sediment core under semiarid recharge rates. Water Resources Research 49, 4985–4996. https://doi.org/10.1002/wrcr.20343

Makarov, M.I., Malysheva, T.I., 2006. Phosphorus in humus acids. Eurasian Soil Sc. 39, 1208–1216. https://doi.org/10.1134/S1064229306110081

Makselon, J., Siebers, N., Meier, F., Vereecken, H., Klumpp, E., 2018. Role of rain intensity and soil colloids in the retention of surfactant-stabilized silver nanoparticles in soil. Environ. Pollut. 238, 1027–1034. https://doi.org/10.1016/j.envpol.2018.02.025

Missong, A., Bol, R., Nischwitz, V., Krüger, J., Lang, F., Siemens, J., Klumpp, E., 2018a. Phosphorus in water dispersible-colloids of forest soil profiles. Plant Soil 427, 71–86. https://doi.org/10.1007/s11104-017-3430-7

Missong, A., Holzmann, S., Bol, R., Nischwitz, V., Puhlmann, H., v. Wilpert, K., Siemens, J., Klumpp, E., 2018b. Leaching of natural colloids from forest topsoils and their relevance for phosphorus mobility. 305 - 315 305.

Mohseni, N., Hosseinzadeh, S.R., Sepehr, A., Golzarian, M.R., Shabani, F., 2017. Variations in spatial patterns of soil-vegetation properties and the emergence of multiple resilience thresholds within different debris flow fan positions. Geomorphology 290, 365–375. https://doi.org/10.1016/j.geomorph.2017.04.023

Molina, F.V., 2016. Soil Colloids: Properties and Ion Binding, 0 ed. CRC Press. https://doi.org/10.1201/b15349

Mörchen, R., Lehndorff, E., Diaz, F.A., Moradi, G., Bol, R., Fuentes, B., Klumpp, E., Amelung, W., 2019. Carbon accrual in the Atacama Desert. Global and Planetary Change 181, 102993. https://doi.org/10.1016/j.gloplacha.2019.102993

Neubauer, E., Schenkeveld, W.D.C., Plathe, K.L., Rentenberger, C., von der Kammer, F., Kraemer, S.M., Hofmann, T., 2013. The influence of pH on iron speciation in podzol extracts: Iron complexes with natural organic matter, and iron mineral nanoparticles. Science of The Total Environment 461–462, 108–116. https://doi.org/10.1016/j.scitotenv.2013.04.076

Ortega, C., Vargas, G., Rojas, M., Rutllant, J.A., Muñoz, P., Lange, C.B., Pantoja, S., Dezileau, L., Ortlieb, L., 2019. Extreme ENSO-driven torrential rainfalls at the southern edge of the Atacama Desert during the Late Holocene and their projection into the 21th century. Global and Planetary Change 175, 226–237. https://doi.org/10.1016/j.gloplacha.2019.02.011

Quade, J., Rech, J.A., Latorre, C., Betancourt, J.L., Gleeson, E., Kalin, M.T.K., 2007. Soils at the hyperarid margin: The isotopic composition of soil carbonate from the Atacama Desert, Northern Chile. Geochemica et Cosmochimica Acta 71, 3772–3795. https://doi.org/10.1016/j.gca.2007.02.016

Rickson, R.J., 2012. Handbook of Soil Sciences. Properties and Processes. Second edition. Edited by P. M. Huang, Y. Li and M. E. Sumner. Boca Raton, FL: CRC Press (2011), pp. 1442, £99.99. ISBN 978-1439803059. - Handbook of Soil Sciences. Resource Management and Environmental Impacts. Second edition. Edited by P. M. Huang, Y. Li and M. E. Sumner. Boca Raton, FL: CRC Press (2011), pp. 830, £89.00. ISBN 978-1439803073. - A two-volume set is also available: pp. 2272, £159.00. ISBN 978-1439803035. Experimental Agriculture 48, 603–604. https://doi.org/10.1017/S0014479712000609

Schelde, K., Moldrup, P., Jacobsen, O.H., Jonge, H. de, Jonge, L.W. de, Komatsu, T., 2002. Diffusion-Limited Mobilization and Transport of Natural Colloids in Macroporous Soil. Vadose Zone Journal 1, 125–136. https://doi.org/10.2113/1.1.125

Séquaris, J.-M., Klumpp, E., Vereecken, H., 2013. Colloidal properties and potential release of water-dispersible colloids in an agricultural soil depth profile. Geofisica Internacional 193, 94–101. https://doi.org/10.1016/j.geoderma.2012.10.014

Séquaris, J.-M., Lewandowski, H., 2003. Physicochemical characterization of potential colloids from agricultural topsoils. Colloids and Surfaces A: Physicochemical and Engineering Aspects 217, 93–99. https://doi.org/10.1016/S0927-7757(02)00563-0

Shang, J., Flury, M., Chen, G., Zhuang, J., 2008. Impact of flow rate, water content, and capillary forces on in situ colloid mobilization during infiltration in unsaturated sediments. Water Resources Research 44, W06411. https://doi.org/10.1029/2007WR006516

Tombácz, E., Csanaky, C., Illés, E., 2001. Polydisperse fractal aggregate formation in clay mineral and iron oxide suspensions, pH and ionic strength dependence. Colloid Polym Sci 279, 484–492. https://doi.org/10.1007/s003960100480

Turner, B.L., Kay, M.A., Westermann, D.T., 2004. Colloidal phosphorus in surface runoff and water extracts from semiarid soils of the western United States. J. Environ. Qual. 33, 1464–1472. https://doi.org/10.2134/jeq2004.1464

Wilkinson, K.J., Lead, J.R., 2007. Environmental Colloids and Particles: Behaviour, Separation and Characterisation. John Wiley & Sons.

Williams, A., Santoro, C.M., Smith, M.A., Latorre, C., 2008. The Impact of Enso in the Atacama Desert and Australian Arid Zone: Exploratory Time-Series Analysis of Archaeological Records. Chungara 40, 245–259.

Zhuang, J., McCarthy, J.F., Tyner, J.S., Perfect, E., Flury, M., 2007. In Situ Colloid Mobilization in Hanford Sediments under Unsaturated Transient Flow Conditions: Effect of Irrigation Pattern. Environ. Sci. Technol. 41, 3199–3204. https://doi.org/10.1021/es062757h

Zhuang, J., Tyner, J.S., Perfect, E., 2009. Colloid transport and remobilization in porous media during infiltration and drainage. Journal of Hydrology 377, 112–119. https://doi.org/10.1016/j.jhydrol.2009.08.011

Supplementary information for

Contrasting depth distribution of colloid-associated phosphorus in the active and abandoned sections of an alluvial fan in a hyper-arid region of the Atacama Desert

Ghazal Moradi[ab], Roland Bol[a], Luka Trbojevic[a], Anna Missong[a], Ramona Mörchen[c], Barbara Fuentes[d], Simon M. May[e], Eva Lehndorff[c], Erwin Klumpp[a]*

[a] Agrosphere (IBG-3), Institute of Bio- and Geosciences, Forschungszentrum Jülich GmbH, Germany

[b] Institute for Environmental Research, Biology 5, RWTH Aachen University, Worringerweg 1, 52074 Aachen, Germany

[c] Institute of Crop Science and Resource Conservation - Soil Science and Soil Ecology, University of Bonn, 53115 Bonn, Germany

[d] Laboratorio de Tecnología de Membranas, Medio Ambiente y Biotecnología, Departamento de Ingeniería Química, Universidad Católica del Norte, Antofagasta, Chile

[e] Institute of Geography, University Cologne, Albertus-Magnus-Platz, 50923 Cologne, Germany

*** Corresponding author:** Ghazal Moradi, g.moradi@fz-juelich.de, Tel: +49 (0)2461613521

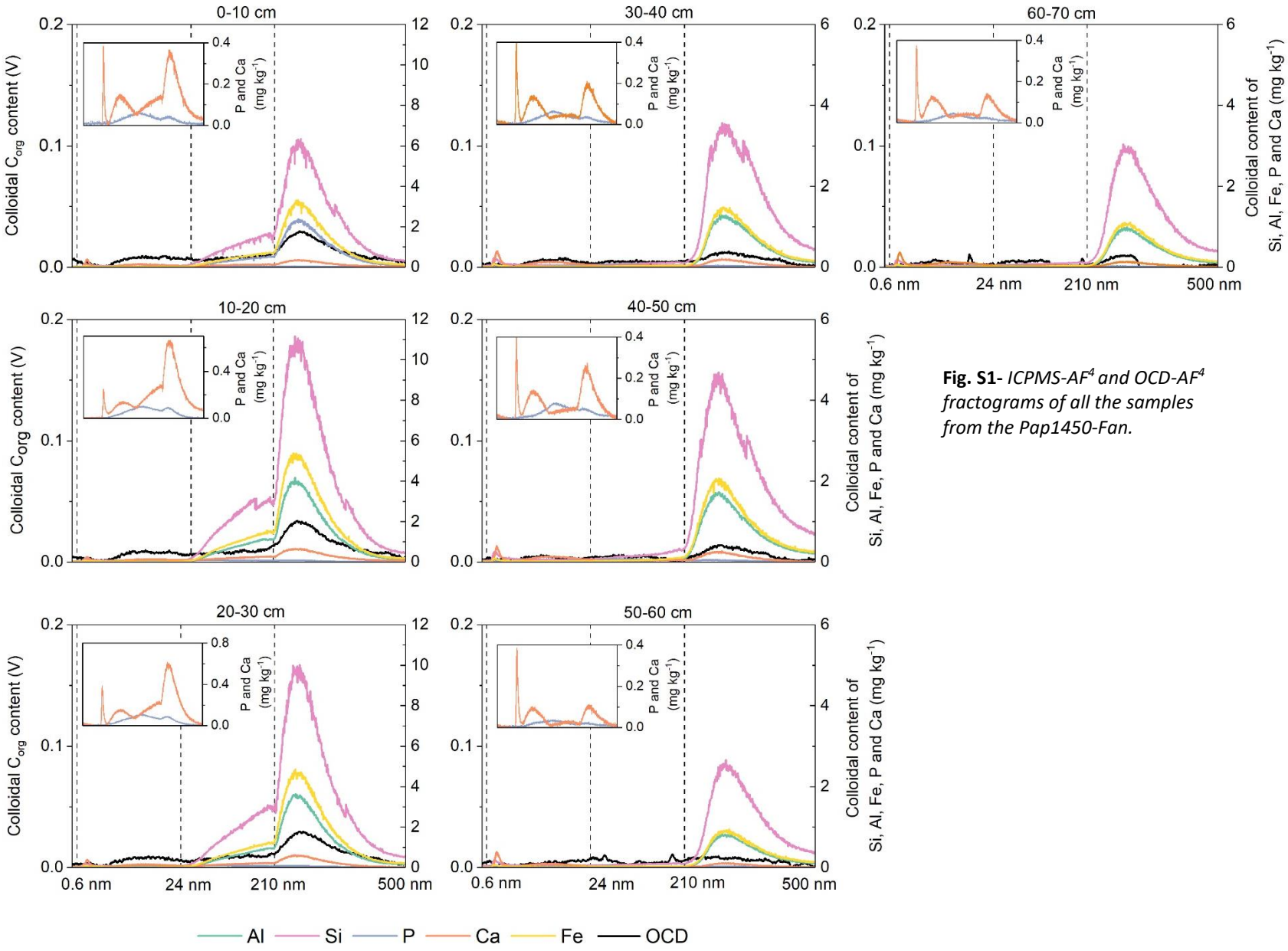

Fig. S1- *ICPMS-AF^4 and OCD-AF^4 fractograms of all the samples from the Pap1450-Fan.*

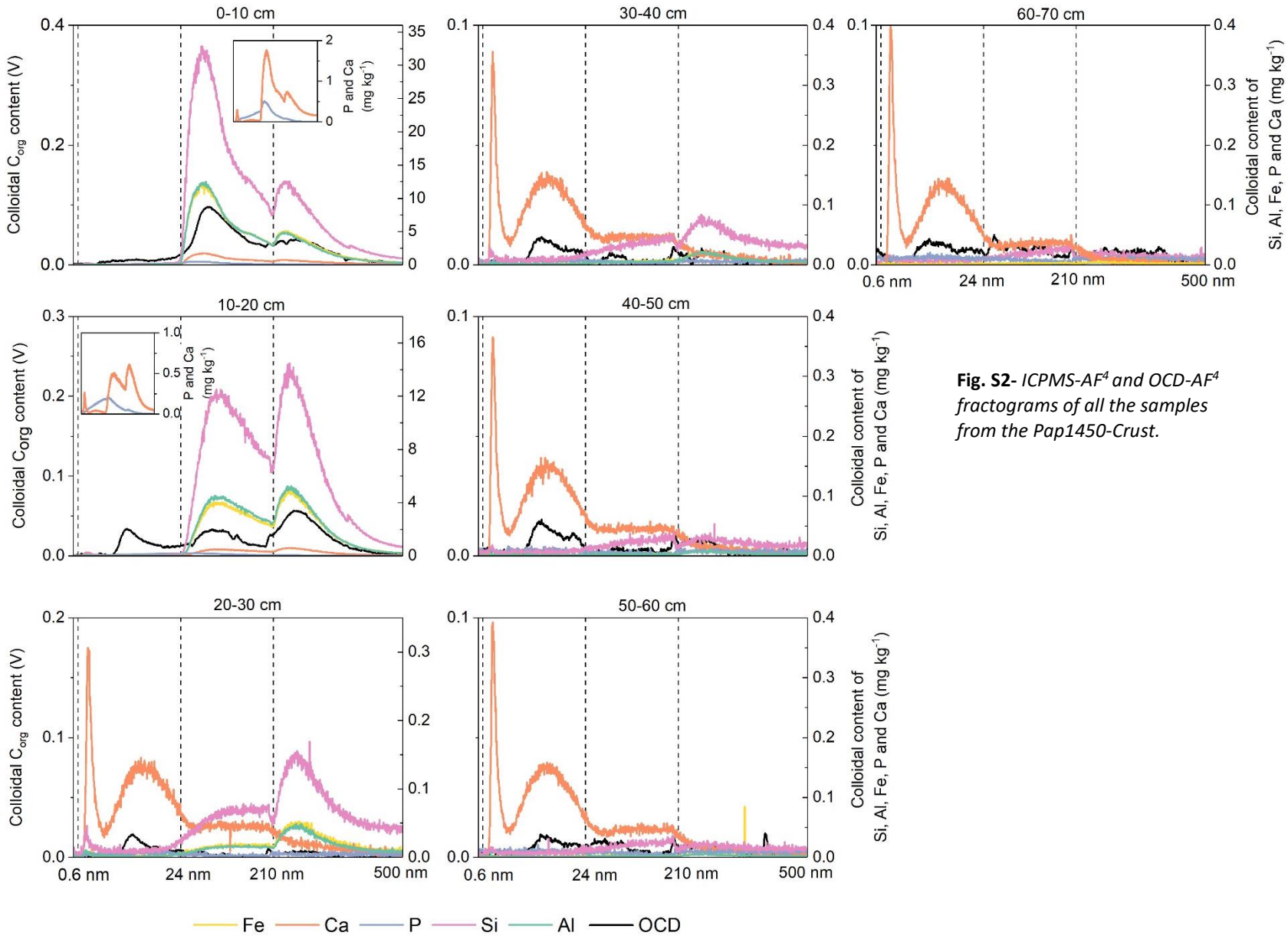

Fig. S2- *ICPMS-AF^4 and OCD-AF^4 fractograms of all the samples from the Pap1450-Crust.*

Table S1- *characteristics of the samples, and element content of WDCs in mg kg^{-1} $_{dry\ soil}$. The average of WDCs is measured by offline DLS measurements. Element concentration of WDCs are calculated from the integrated peak areas of fractograms. Also, the elemental content of NP, FC and MC are given.*

Profile	depth	pH	DLS	total OC*	total P	Si			Fe			Al			P			Ca			OC		
	cm		nm	mg/kg	mg/kg	mg/kg			mg/kg			mg/kg			mg/kg			mg/kg			mg/kg		
						NP	FC	MC	NP	FC	MC	NP	FC	MC	NP	FC	MC	NP	FC	MC	NP	FC	MC
Pap1450-Crust	0-10	8.3	296	450	1688	0.7	354.1	145.1	0.2	132.2	58.6	0.2	134.6	54.6	0.2	5.5	0.6	0.4	19.7	10.2	0.3	3.1	1.8
	10-20	8.8	304	455	2511	0.6	163.9	155.8	0.2	53.7	54.1	0.1	59.5	56.8	0.1	2.5	0.4	0.4	7.4	9	0.7	1.1	2
	20-30	8.6	341	495	1662	0.1	1.1	2.2	0	0.3	0.7	0	0.3	0.6	0	0.1	0.1	0.6	1.8	2.4	0	0.5	0.2
	30-40	8.5	306	470	1525	0.6	1.6	46.7	0.2	0.5	17.6	0.1	0.2	15.5	0	0.8	0.6	0.7	2	5.7	0	0.3	0.2
	40-50	8.5	300	460	1323	0	0.4	0.6	0	0.1	0.1	0	0.1	0.1	0	0.1	0.2	0.6	1.9	2.6	0	0.4	0.3
	50-60	8.5	317	500	1345	0.5	1.4	32.5	0.2	0.4	11.6	0.1	0.2	10.1	0	0.4	0.4	0.6	1.5	4.3	0	0.4	0.3
	60-70	8.5	311	495	1407	0	0.3	0.4	0	0	0.1	0	0	0.1	0.1	0.1	0.3	0.7	1.5	2.4	0	0.6	0.4
Pap1450-Fan	0-10	8.1	318	445	1428	0.5	16.5	72.5	0.2	7.2	35.5	0.1	5.2	26	0.1	0.8	0.5	0.4	1.7	4.3	0.4	0.3	1.3
	10-20	8	352	605	1708	0.5	33.6	123.1	0.2	14.8	58.1	0.1	11.4	43.8	0	1.5	1	0.4	3.3	8.3	0.4	0.3	1.4
	20-30	8.1	364	435	1586	0.6	28.8	112.6	0.2	11.8	52.3	0.1	9.1	39.6	0	1.5	1	0.6	4.2	10.8	0.3	0.4	1.3
	30-40	8.1	412	415	178	0.6	1.6	46.7	0.2	0.5	17.6	0.1	0.2	15.5	0	0.8	0.6	0.7	2	5.7	0.2	0.2	0.6
	40-50	8.1	415	415	1875	0.6	3	62	0.2	0.9	25.3	0.1	0.6	21.6	0	1.1	0.9	0.6	2.2	6.8	0.1	0.2	0.6
	50-60	8	424	455	1552	0.5	1.4	32.5	0.2	0.4	11.6	0.1	0.2	10.1	0	0.4	0.4	0.6	1.5	4.3	0	0.3	0.6
	60-70	7.6	398	405	1404	0.5	1.4	36.8	0.2	0.4	13.4	0.1	0.2	11.7	0	0.6	0.4	0.6	1.8	4.9	0.1	0.2	0.2

** Total OC content of bulk soils are taken from (Mörchen et al., 2019)*

Table S2- *Parameters of the AF^4 separation method.*

Parameters	
Detector flow	0.5 mL min^{-1}
Injection volume	500 µL
Spacer	500 µm
Membrane	1kDa PES
Carrier solution	25 µM NaCl
Focus time	6 min
Transition time	0.5 min
Cross-flow $t_{0\ min} - t_{6\ min}$	3 mL min^{-1}
Cross-flow $t_{6\ min} - t_{6,5\ min}$	3 mL min^{-1}
Cross-flow $t_{6,5\ min} - t_{10\ min}$	1.98 mL min^{-1}
Cross-flow $t_{10\ min} - t_{17\ min}$	1 mL min^{-1}
Cross-flow $t_{17\ min} - t_{20\ min}$	0.7 mL min^{-1}
Cross-flow $t_{20\ min} - t_{26\ min}$	0.15 mL min^{-1}
Cross-flow $t_{26\ min} - t_{35\ min}$	0.07 mL min^{-1}
Cross-flow $t_{46\ min} - t_{111\ min}$	0 mL min^{-1}

Reference:

Mörchen, R., Lehndorff, E., Diaz, F.A., Moradi, G., Bol, R., Fuentes, B., Klumpp, E., Amelung, W., 2019. Carbon accrual in the Atacama Desert. Global and Planetary Change 181, 102993. https://doi.org/10.1016/j.gloplacha.2019.102993